Title
Deep clinical and neuropathological phenotyping of Pick disease

Journal
Annals of Neurology, 79(2)

ISSN
0364-5134

Authors
Irwin, David J
Brettschneider, Johannes
McMillan, Corey T
et al.

Publication Date
2016-02-01

DOI
10.1002/ana.24559

Peer reviewed

HHS Public Access

Author manuscript

Ann Neurol. Author manuscript; available in PMC 2017 February 01.

Published in final edited form as:

Ann Neurol. 2016 February ; 79(2): 272–287. doi:10.1002/ana.24559.

Deep Clinical and Neuropathological Phenotyping of Pick's Disease

David J. Irwin[1,2,*], **Johannes Brettschneider**[5,*], **Corey T. McMillan, PhD**[1], **Felicia Cooper, MS**[1,2], **Christopher Olm, MS**[1], **Steven E. Arnold, MD**[3], **Vivianna M. Van Deerlin, MD, PhD**[2], **William W. Seeley, MD**[6], **Bruce L. Miller, MD**[6], **Edward B. Lee, MD, PhD**[2,4], **Virginia M.-Y. Lee, PhD, MBA**[2], **Murray Grossman, MD**[1], and **John Q. Trojanowski, MD, PhD**[2]

[1]University of Pennsylvania Frontotemporal Degeneration Center, Department of Neurology, University of Pennsylvania, Philadelphia, PA 19104, USA

[2]Center for Neurodegenerative Disease Research Department of Pathology and Laboratory Medicine, University of Pennsylvania, Philadelphia, PA 19104, USA

[3]Brain-Behavior Laboratory, Department of Psychiatry, Perelman School of Medicine, University of Pennsylvania, Philadelphia, PA 19104, USA

[4]Translational Neuropathology Research Laboratory, University of Pennsylvania, Philadelphia, PA 19104, USA

[5]Department of Neurology, Klinikum-Herford, Germany

[6]Memory and Aging Center, Department of Neurology, University of California, San Francisco

Abstract

Objective—To characterize sequential patterns of regional neuropathology and clinical symptoms in a well-characterized cohort of 21 patients with autopsy-confirmed Pick's disease.

Methods—Detailed neuropathological examination using 70 μm and traditional 6 μm sections was performed using Thioflavin-S staining and immunohistochemistry for phosphorylated-tau, 3R and 4R tau isoforms, ubiquitin, and C-terminally truncated tau. Patterns of regional tau deposition were correlated with clinical data. In a subset of cases (n=5) converging evidence was obtained using antemortem neuroimaging measures of grey and white matter integrity.

Results—Four sequential patterns of pathological tau deposition were identified starting in frontotemporal limbic/paralimbic and neocortical regions (Phase I). Sequential involvement was seen in subcortical structures, including basal ganglia, locus coeruleus and raphe nuclei (Phase II),

Please send correspondence to: David J. Irwin, MD, Frontotemporal Degeneration Center/Center for Neurodegenerative Disease Research, University of Pennsylvania Perelman School of Medicine, Hospital of the University of Pennsylvania, 3600 Spruce Street, Philadelphia, PA 19104, (215)-662-3361 dirwin@mail.med.upenn.edu.

*These authors contributed equally

Potential Conflicts of Interest

The authors declared no potential conflicts of interest with respect to the research, authorship, and/or publication of this article.

Author Contributions

JB, DJI, MG, VMYL, JQT provided conception and design of the study. JB, DJI, CTM, CO, SEA, VMVD, WWS, BLM, EBL, MG, JQT provided acquisition and analysis of data. DJI drafted the manuscript and figures. DJI, CMT, MG, VMYL, JQT provided funding. JB, DJI, CTM, CO, VMVD, WWS, BLM, MG and JQT provided critical revisions of the manuscript.

followed by primary motor cortex and pre-cerebellar nuclei (Phase III) and finally visual cortex in the most severe (Phase IV) cases. Behavioral variant frontotemporal dementia was the predominant clinical phenotype (18/21) but all patients eventually developed a social comportment disorder. Pathological tau phases reflected the evolution of clinical symptoms and degeneration on serial antemortem neuroimaging, directly correlated with disease-duration and inversely correlated with brain-weight at autopsy. The majority of neuronal and glial tau inclusions were 3R tau-positive and 4R tau-negative in sporadic cases. There was a relative abundance of mature tau pathology markers in frontotemporal limbic/paralimbic regions compared to neocortical regions.

Interpretation—Pick's disease tau neuropathology may originate in limbic/paralimbic cortices. The patterns of tau pathology observed here provide novel insights into the natural history and biology of tau-mediated neurodegeneration.

Introduction

The term "Pick's disease" (PiD), named after Arnold Pick for his initial description of focal gross atrophy of the frontotemporal lobes in a patient with progressive language and behavioral disturbances [1], has undergone several paradigm shifts as a clinicopathological entity [2]. According to modern nomenclature [3], PiD corresponds to a form of tauopathy consisting of spherical intra-neuronal tau inclusions composed predominately of tau isoforms containing three microtubule binding domain (MTBD) repeats (i.e. 3R tau). As such, PiD is a member of the frontotemporal lobar degeneration (FTLD) spectrum of neurodegenerative tauopathies (i.e. FTLD-Tau) [3] and is associated with several clinical frontotemporal dementia (FTD) syndromes. Indeed, PiD is most commonly associated with a disorder of social comportment and executive impairments [4, 5], known as the behavioral-variant of FTD (bvFTD) [6], but also can manifest as a progressive disorder of language [5] (i.e. primary progressive aphasia; PPA) [7] or less commonly an akinetic-rigid syndrome with executive, praxis, and visuospatial deficits (i.e. corticobasal syndrome; CBS) [8].

Here we use complementary immunohistochemical (IHC) and histochemical techniques to describe the patterns of regional neuropathological burden in a series of patients with PiD of varying severities and relate these apparent phases to clinical and multi-modal neuroimaging data. Our goal was to provide a deep phenotypic profile of neuropathological progression of PiD tauopathy and relationship to clinical FTD symptoms.

Methods

Patients

Patients were selected from the University of Pennsylvania (Penn) Perelman School of Medicine brain bank at the Center for Neurodegenerative Disease Research (CNDR) with a primary neuropathological diagnosis of PiD (n=21). Cases were followed clinically at the Penn Frontotemporal Degeneration Center, Penn Alzheimer's Disease Center, or University of California San Francisco Memory and Aging Center. All procedures were performed with informed consent in accordance with local Institutional Review Board guidelines. Neuropathological diagnosis was performed by an experienced neuropathologist (JQT,

EBL) using previously described methods [9] and diagnostic criteria [3, 10]. Two cases (one previously reported [11]) had a p.Leu266Val pathogenic mutation in *MAPT* [11]; This mutation is associated with 3R tau Pick bodies with morphology indistinguishable to sporadic disease [11, 12] and thus, included for study.

Tissue Preparation and IHC

Fresh samples from standard regions [9] were obtained and fixed overnight in either 70% ethanol with 150 mM NaCl or 10% neutral buffered formalin and embedded in paraffin blocks. Postmortem interval to fixing ranged from 4–42 hours (mean=15.6±13.8). Available tissue for each case was examined using both traditional 6 μm sections and thick 70 μm paraffin-embedded sections, as described [9, 13]. Two cases were studied using 6 μm sections only. Free-floating 70 μm thick sections were stained with aldehyde fuchsin and Darrow Red to visualize neuronal cell bodies and IHC with a well-characterized phospho-specific tau monoclonal antibody (MAb) (i.e. AT-8; Thermo Scientific, Waltham MA) [14] as described [13, 15]. This technique allows for increased visualization of neuropathology and enhances study of neuroanatomic structures.[13, 15] Standard 6 μm sections were stained with Thioflavin-S (ThS) to detect tau inclusions with amyloid-dye binding properties, and IHC using primary MAbs specific for phospho-tau (12E8; Elan Pharmaceuticals, San Francisco, CA)[16], ubiquitin (UBQ) (1510; Millipore Billerica, MA) [17], 4R tau (RD4; Millipore[18]; Anti-4R Tau; (Cosmo Bio, Carlsbad, CA)[19], and C-terminally truncated tau (TauC3; Dr. LI Binder) [20] using methods as described [9, 21, 22]. Finally, double-label immunofluorescence experiments were performed using AT-8, RD4 or 3R tau (RD3; Millipore) [18] with MAbs specific for glial fibrillary associated protein (GFAP; Dako Carpinteria, CA) [23] or microtubule-associated protein 2 (MAP2) (17028; CNDR) [24] and Alexa Fluor 488 and 594 species-specific secondary antibodies (Molecular Probes) as described [21, 22]. A Leica SPE confocal microscope was used to confirm signal co-localization (Leica Microsystems, Buffalo Grove, IL).

Microscopic Analysis

70 μm sections were independently examined by experienced investigators (JB, DJI) and graded on a standard validated ordinal scale (i.e. 0=none/rare, 1=mild, 2=moderate, 3=severe)[10, 15, 25] for the burden of tau deposition and neuronal loss in the following regions: amygdala (AMY), hippocampus (HIPP), orbitofrontal cortex (OFC), mid-frontal cortex (MFC), anterior cingulate gyrus (ACG), superior/mid-temporal gyri (SMT), primary motor cortex (MOT), angular gyrus (ANG), primary sensory cortex (SENS), primary visual cortex (VIS), caudate nucleus and putamen (striatum STR), globus pallidus (GP), thalamus (THAL), midbrain, pons, medulla (MED), cerebellum (CB) and cervical spinal cord (CSC). Anatomic regions/nuclei within these sections examined included: the cornu ammonis/ subiculum (CA), entorhinal cortex (ERC) and dentate gyrus (DG) in HIPP; substantia nigra (MBSN) and red nucleus (MBRN) in midbrain; locus coeruleus (LC) and raphe nuclei (RPN) in the pons; hypoglossal nucleus (MEDXII), dorsal motor nucleus of the vagus (MEDX), reticular formation (MEDRF), inferior olive (MEDIO), and arcuate nucleus and pontobulbar body pre-cerebellar nuclei (MED ARC/PB); dentate nucleus (CBDG) and granular layer (CBGL) of the cerebellum. Discrepant scores were re-reviewed by both examiners and consensus scores were reached. Sections were also separately graded for the

severity of ramified astrocytes and tau pathology in adjacent white matter (WM). Finally, since PiD can preferentially affect specific cortical lamina (i.e. II, VI) [26], cortical sections were also examined for tau deposition in superficial cortical layers (layers II-III) and deep cortical layers (V-VI). Hypothetical phases of sequential tau deposition were constructed through comparison of regional involvement for AT-8 staining in 70 μm thick sections.

A subset of regions (AMY, ERC, DG, CA, MFC, OFC, ACG, SMT, ANG, SENS, STR, MOT, VIS) were selected for 6 μm section IHC experiments for UBQ, ThS, Tau C3, RD4 and anti-4R tau and graded on a similar ordinal scale.

Clinical Analysis

Clinical data was extracted by an experienced cognitive neurologist (DJI) to capture the reported year of onset of core clinical symptoms of bvFTD [6] (i.e. executive dysfunction, behavioral disinhibition, apathy/inertia, loss of sympathy/empathy, ritualistic behavior, hyper-orality) and neuropsychiatric symptoms from the history. Symptoms reported to be present as part of the initial clinical presentation were counted as having 0 years from onset. When no clear onset date could be determined, the visit date of the symptom report was used. Clinical signs were recorded from the visit date when detected by examination including deficits in: episodic memory, visuospatial function, limb praxis, non-fluent speech, language comprehension (single word/object or sentence level), speech repetition, naming and extrapyramidal features (bradykinesia and/or rigidity). Episodic memory loss was recorded when there was poor recall and recognition of verbal/visual stimuli (i.e. encoding deficit). Non-fluent speech was recorded when speech was reported as slow or hesitant, and dysarthric speech was noted separately. All cases had ≥1 center visit for evaluation. Earliest available ante mortem neuropsychology scores were obtained from the Penn Integrated Neurodegenerative Disease Database[9].

Neuroimaging Analysis

Ante mortem magnetic resonance imaging (MRI) data were available for five patients (Supplementary Tables 11–12). MRI data was processed using ANTS normalization tools as described [27]. We measured GM density in 15 regions of interest (ROIs) constrained to encompass anatomical areas sampled at autopsy (listed above) and identified in an aging atlas comprised of OASIS data and parcellated using multi-atlas label fusion (MALF). We also measured mean diffusivity (MD) for WM integrity in ROIs from a standardized atlas [28]. Since there was random sampling of hemispheres in our autopsy series we averaged the left and right hemisphere data. For the first and last available MRI, we report the average z-score <−2.0 from all patients in predefined ROIs that were generated relative to a demographically comparable aging cohort comprised of 60 healthy controls (31 female, 29 male) screened for negative self-report of psychiatric or neurological history: Mean Age = 62.67 (7.49); Mean Education = 15.67 (2.29).

Statistical Analysis

Comparisons of ordinal pathology score ratings were performed using non-parametric Kruskal-Wallis, Mann-Whitney U and Spearman Correlation statistics. Categorical variables were compared using a chi-squared analysis. All analysis were two-sided with α=0.05 with

the exception of comparison of mature tau markers between regions which we used α=0.001 to correct for multiple comparisons. Statistics were performed using SPSS version 21.0 (IBM Corp., Armonk NY) or Graph Pad Prism v4.01 (Graphpad software, La Jolla, CA).

Results

PiD neuropathology

Examination of 70 μm thick sections revealed a varying degree of tau-positive pathological inclusions throughout the central nervous system (CNS) (Figure 1). Consistent with the neuropathological diagnosis of PiD [26] the most predominant morphology was intra-neuronal spherical Pick bodies (PBs) (Figure 2). These were most conspicuous in the hippocampal DG and upper cortical layers (II-III) of frontal and temporal neocortical regions. PB were also variably present in lower cortical layers (V-VI). We did not observe isolated involvement of lower cortical layers, and the MFC and ACG consistently had both superficial and deep layer distribution of PBs in all cases (Supplementary Table 4). Diffuse, tau-positive neuropil threads (NTs) were often found in association with PBs and swollen weakly tau-positive ballooned neurons were most obvious in limbic cortex (ACG, AMY) but were present to varying degrees in affected neocortex. Ramified astrocytic tau inclusions (Figure 2H) were found in most cases and were most prominent in MFC and OFC. The majority of inclusions with this morphology co-localized, or partially co-localized, to GFAP and not MAP2 (Figure 3A–B) confirming astrocytic origin. Ordinal tau pathology GM scores were highly correlated with scores for neuronal loss in most cortical/limbic regions (AMY, ERC, OFC, MFC, ACG, SMT, ANG, MOT, SENS rho= 0.7–0.9, $p<0.003$). In regions/cases with mild tau pathology there was often no appreciable neuronal loss; this was most obvious in the visual cortex. WM tau pathology appeared to be prominent both in axons and adjacent oligodendrocytes (Figure 2D, I). Both oligodendrocytes near neuronal soma in GM (i.e. satellite oligodendrocytes) and also in WM often contained tau-positive coiled inclusions (Figure 2I–J) Less commonly, rounded oligodendroglial tau inclusions resembled small Pick-bodies.[29] Ordinal scores for WM tau inclusions seldom were more severe than adjacent GM in neocortical/limbic cortex (Supplementary Table 3) and both were highly correlated (rho=0.6–0.8, $p<0.03$; OFC, MFC, ACG, MOT, SENS, SMT, ANG). Layer V-VI involvement was also correlated with higher WM tau pathology scores (rho=0.6–0.9, $p<0.02$; OFC, SMT, MOT, SEN, ANG; MFC and ACG cannot be calculated since all cases uniformly had both superficial and deep layer tau pathology).

Conflicting reports exist for 12E8 MAb reactivity in PiD[30, 31], which marks the phospho-epitopes Ser262/356 in the MTBDs. We found moderate to strong reactivity for 12E8 in all sporadic and *MAPT* p.L266V cases (Figure 3G). Finally, PiD is largely a 3R tauopathy; however, a subset of cases may have varying degrees of insoluble 4R tau pathology [21, 30]. As such, we screened these regions for reactivity to two different 4R specific tau MAb (RD4, anti-4R tau). We found a subset of cases (8/19 sporadic, Supplemental Tables 8,9) with mild amounts of 4R-positive tau pathology which was largely in PBs (Figure 3H). Areas of moderate 4R-positive tau pathology were rare, and in these instances 4R tau astrocytic inclusions were also present to varying degrees in proximity to 4R-positive tau PBs. In contrast, the p.Leu266Val *MAPT* mutation cases consistently had punctate 4R-tau

positive glial inclusions throughout the CNS without the presence of 4R-reactive PBs (Figure 3I), similar to previous reports [11, 12]. In sporadic cases, double-labelling experiments found astrocytic inclusions were 3R tau-positive (Figure 3C) and not 4R tau-positive (Figure 3D). There did not appear to be a relationship of severity of pathology to the presence of 4R tau.

Phases of PiD Neuropathology

Four sequential patterns of regional pathology emerged through comparison of the PiD cases examined (Figures 1,4):

Phase I. The single Phase I case showed a moderate to severe burden of tau pathology in limbic regions (AMY, ERC, DG, CA, ACG) and frontotemporal neocortex (OFC, MFC, SMT). Milder involvement of ANG was seen in this case and in all other cases.

Phase II. Three cases made up an apparent second phase of increasing tau pathology distribution. Regions affected in this phase but not the Phase I case included subcortical structures including the STR, THAL, MBSN, MBRN, LC, RPN, MEDX, MEDRF and primary SENS. LC and RPN showed consistent moderate to severe intracellular tau inclusions (Figure 5E–G) in all but the most mildly affected case. These appeared to localize to dendrites and neuronal perikarya (Figure 3F). Phase II cases also had tau pathology in the CSC and CBDG. Spinal cord pathology was most concentrated in upper Rexed layers with rare involvement of lower motor neurons in Rexed layer VIII-IX (Figure 5A–D).

Phase III. Phase III cases had tau pathology extending further into additional regions including primary MOT and medullary pre-cerebellar nuclei (MEDIO, MEDARC/PB). Pre-cerebellar nuclei, including the inferior olivary nucleus showed dot-like stippling patter of tau reactivity (Figure 5H).

Phase IV. Finally the PiD cases with the most severe and widespread tau pathology (Phase IV) were defined by extension of tau pathology into the primary visual cortex without appreciable neuron loss. VIS tau pathology appeared as spherical intraneuronal PBs with varying degrees of large diffuse astrocytic tau inclusions (Figure 5I). Rare involvement of the CBGL and MEDXII was seen at this phase as well.

WM tau pathology largely followed this sequential phasing scheme (Figure 4, Supplemental Table 3) with rare or absent WM tau pathology in the mild Phase I case. There was variable moderate to severe tau pathology in neocortical- and limbic-associated WM in Phase II cases. MOT WM tau pathology was present only in Phase III-IV cases. Mild to moderate WM tau pathology was seen in WM in SENS, CB, midbrain crus cerebri and medullary pyramids in Phase IV cases only. There was rare or absent VIS WM tau pathology.

Clinical features

Patient demographics and neuropathological findings are listed in Figure 1. Mean age at onset was 57.0±12.5, mean age of death was 65.5±13.4 and mean disease duration was 8.6±3.9 years. The p.Leu266Val *MAPT* mutation cases (cases #17,21) had a much earlier ages of onset and death with disease duration similar to the average for the group (8, 5

years). The majority of patients (18/21) initially presented with a social comportment disorder consistent with modern criteria for bvFTD [6] (Supplementary Table 10). Two patients had a parietal lobe syndrome with apraxia and extrapyramidal features consistent with CBS [32], one of whom also had 2/5 core bvFTD symptoms within the first three years of disease (case #13), while the other patient had prominent motor speech difficulties consistent with the non-fluent variant of PPA (naPPA) [7] and later also developed 3/5 core features of a social comportment disorder (case #6). One case presented with episodic memory loss and a social comportment disorder; as such, a diagnosis of AD was given with mention of "possible PiD" (case #16). Finally, one bvFTD patient also had significant dysarthria and bulbar weakness. FTD-ALS was considered as a clinical diagnosis but an EMG-NCV was negative for motor neuron disease (case #14).

The onset of clinical symptoms and signs from the clinical record are listed in Supplementary Table 10. The mean interval from reported onset to first visit was 3.3 years and the mean interval from last visit to death was 3.3 years. As expected, the majority of cases had evidence for a social comportment disorder, largely within the first three years of reported symptoms. Loss of empathy was less frequently reported than other behavioral symptoms (11/21 cases vs 17–21/21 cases). Episodic memory loss was detected eventually in 11/21 cases but only as a presenting feature in five cases. Visuospatial dysfunction occurred on average five years after onset and was less common (8/21 cases) but was present in both CBS cases. There was a varying degree of language problems detected in the record with word-finding difficulty (10/21 cases) and naming problems (12/21 cases) being the most common. Non-fluent speech was less common (7/21 cases) and rare within the first three years of symptoms (3/21 cases). Single word and sentence-level language comprehension also was present in 10/21 of cases but was less common early in the disease (4/21 cases). Finally a large number of patients (14/21 cases) were noted to develop extrapyramidal features during the course of their disease, but this was a relatively late phenomenon (mean= 4.5 years after onset). Neuropsychiatric symptoms were rare and included one patient who developed delusions of snakes or children in the house and another who had auditory hallucinations. The subset of cases with neuropsychological data (n=14) show largely mild to moderate global impairment at first visit with specific impairment in working memory (i.e. digits forward), executive functioning (i.e. digits backwards) and mild naming difficulty (i.e. Boston naming test).

Clinicopathological Correlations

The increasing extent of tau pathology from Phases I-IV was associated with an increased ordinal score of tau pathology burden for most regions (rho=0.6–0.8, $p<0.01$ AMY, CA, ACG, STR, MOT, VIS). Cases with missing VIS 70μm thick section data (#18–21) were classified as Phase IV due to a high burden of tau inclusions in pre-cerebellar nuclei. Notably, the tau phases described above directly correlated with disease duration (rho=0.5, $p=0.03$) and inversely correlated with brain weight at autopsy (rho=−0.6, $p=0.01$) in sporadic cases. The *MAPT* p.Leu266Val cases had a very severe burden of pathology (both similar to Phase IV). PiD patients diagnosed clinically with CBS had Phase III or IV tau pathology with no clear difference in tau pathology burden in basal ganglia or parietal lobes compared with bvFTD cases in the same phase. Case # 14 with bulbar symptoms who was

considered to have clinical ALS-FTD had available tissue in the thoracic, lumbar and sacral spinal cord which showed a rostro-caudal gradient of rare-to-mild lower motor neuron tau inclusions, with the highest severity in medullary and pontine cranial nerve motor nuclei. Visuospatial difficulties and extrapyramidal features occurred relatively late in the disease course on average (~5 years) and occurred only in cases ≥ Phase II pathology at autopsy, which includes tau inclusions in ANG, GP, STR and MBSN.

Examination of Phase I Regions with Mature Tau Markers

Several regions were involved in Phase I (Figure 1) and mean ordinal scores using AT-8 reactivity found a ceiling effect across regions making qualitative differences between regions difficult to detect (Figure 6A). In an effort to further delineate the sequential regional deposition of tau in Phase I regions, we examined several markers of more mature tau pathology. Indeed, tau undergoes a sequential progression of modifications including phosphorylation, acetylation and C-terminal truncation, during tangle formation from “pre-tangles” to tau tangles that bind amyloid dyes across tauopathies. Some of these modifications, such as C-terminal truncation and ThS reactivity, are less abundant or absent in less mature tangles in AD and other tauopathies [20–22, 33–35]; mature tau markers are more common in the hippocampus (an early stage region) in AD cases, especially in advanced cases, suggesting that an area with higher accumulation of these markers may be an early locus of disease [20, 22]. Thus, we examined ThS reactivity in regions that defined Phases I-IV (Figure 1) and found mild to moderate ThS reactivity in PBs that was most obvious in the dentate layer of the hippocampus (Figure 6B, 7D).

Next, we examined the Tau C3 MAb, which recognizes a C-terminal truncation epitope present in NFTs and ghost tangles in AD [20] and a subset of PBs in PiD [34] and thus, is also considered a marker of mature tau pathology [20, 22]. We found a subset of PBs were reactive to Tau C3. These were most obvious in DG and upper layer of neocortical regions (Figure 7E, H). We observed a regional gradient where limbic/paralimbic regions and also OFC and MFC, which define Phase I, had higher levels of Tau C3 reactivity compared to other regions (Figure 6C).

Next, we examined UBQ staining as a subset of PBs have been described to be UBQ+ and the level of UBQ reactivity was mild in a case of pre-symptomatic PiD [36], which suggested that ubiquitination of PBs occurs later in the progression of PiD pathology. The case with minimal pathology classified as Phase I (case #1) had minimal amounts of these mature pathology markers in any region (Figure 7A–C; Supplemental Tables 5–7). Further, we found higher levels of UBQ+ PBs in limbic regions across all cases (Figure 6D, 7F, I, L). In sum, these markers suggested that HIPP, AMY and ACG may be early sites of tau pathology

Neuroimaging features

Five cases had ≥1 ante mortem MRI images available for study. We compared ROIs that encompass GM and WM regions sampled at autopsy and compared to healthy controls in serial MRI scans to further investigate sequential phases of neurodegeneration linked to tau pathology at time points preceding autopsy (Figure 8). The average years from disease onset to baseline MRI was 4.4 (range 0–6) and average years from follow-up MRI to death was

7.8 (range 4–9). Similar to our pathologically-defined tau phases, we find early and severe MRI changes in limbic/paralimbic regions including AMY, ACG and to a lesser degree HIPP/ERC. The insula, though not specifically sampled for histology, also showed severe and progressive atrophy on MRI. Neocortical frontal regions (OFC, MFC) were similarly atrophic and STR mildly affected. Emergence of atrophy in subsequent scans largely aligned with the phases of tau neuropathology with additional SMT involvement and absence of VIS atrophy. There was relatively minimal atrophy of SENS, ANG, GP and THAL with only mild MOT atrophy on follow up scans. MD measurements of WM tracts found similar early and progressive involvement of limbic and frontal association tracts and sparing of motor pathways and optic radiations (Figure 8).

Discussion

Here we characterized four patterns of increasing pathological tau inclusion burden through detailed examination using methods that are sensitive for detecting mild pathologyin one of the largest clinical-pathological studies of PiD: Phase I starting in frontotemporal limbic/neocortex and angular gyrus; Phase II extension into subcortical basal ganglia, brainstem noradrenergic/serotonergic nuclei, cerebellar dentate nucleus and sensory tracts of the spinal cord; Phase III with further involvement of primary motor cortex and pre-cerebellar nuclei; Phase IV with additional mild degree of tau deposits in primary visual cortex. We correlated this phase scheme with antemortem clinical symptoms and neuroimaging. Finally, we find that limbic/paralimbic cortex in the HIPP, AMY and ACG have a higher burden of mature tau pathology markers than other regions that define Phase I, suggesting these sites may be among the earliest to undergo tau deposition in PiD.

Similar to previous reports [4, 5], the majority of patients had an initial clinical phenotype consistent with bvFTD. Indeed, all patients had ≥2 features of social comportment disorder reported, suggesting social disorder is a prominent manifestation of PiD neuropathology. In contrast to previous reports [4, 5], we found only a single patient that met clinical criteria for PPA (with CBS); language features were common during the course of disease but non-specific for PPA. Episodic memory difficulty was present in roughly half of the patients, similar to another series [5], but was often a relatively late finding despite the heavy early burden of tau pathology observed in the hippocampus. This discrepancy is intriguing and memory loss in bvFTD may arise in part due to disease involving prefrontal and hippocampal regions [37]. This is a retrospective assessment from the clinical record, and we cannot conclude that the absence of report of a symptom is definitive evidence that this feature was not present during life.

The phase patterns of tau pathology suggested here are preliminary and do not represent true hierarchical staging as there were few cases with mild pathology. Indeed, we did not have access to “incidental” pre-symptomatic cases of PiD, which are exceptionally rare; however, the patterns of pathology in these few reported cases [36, 38–40] are similar to our Phase I case. Interestingly, the absence of WM tau pathology in this case suggests PiD may originate in GM. The presence of mild ANG tau pathology in absence of MOT and SENS in this case is somewhat surprising as parietal lobe involvement is usually less prominent in PiD[8]; however, our methods are more likely to detect mild amounts of pathology[13]. It is tempting

to speculate that ANG tau pathology in the Phase I case could be the result of propagation of pathological tau along deep WM association tracts not sampled in the current study. Systematic WM sampling will be important for future staging efforts.

To further delineate the earliest involved regions we examined several markers of mature PiD pathology (i.e. ThS, TauC3, UBQ) and hypothesized that increased reactivity for these mature tau markers in a region may indicate an earlier locus of disease, as previously proposed by others [20, 34]. Indeed, we found there was a higher burden of these markers in limbic/paralimbic regions (HIPP, AMY, ACG) than neocortical regions (Figure 6B–D). It is impossible to retrospectively determine the exact loci of early tau deposition in PiD; however, these results suggest limbic/paralimbic cortex may be intimately involved in the origins of PiD. Indeed, neuroimaging data stratified by clinical disease stage [41] finds the anterior insula and cingulate cortex are an early areas of degeneration of bvFTD, and several studies highlight selective vulnerability of specialized neurons important for emotional processing found in these regions [42, 43]. We examined adjacent anterior insula on GP slides (present in 7 cases, including Phase I case), all of which had moderate to severe burden of tau pathology and using MRI (Figure 8). Thus, these data reinforce the importance of the paralimbic network in the origins of bvFTD.

We also confirmed our previous findings[30] with consistent 12E8 reactivity in all cases. Others have claimed that an absence of 12E8 reactivity in PiD.[31] Tissue processing methods may explain this discrepancy as we use a time-limited fixation period of ~24 hours for freshly dissected CNS tissue blocks for fixation[9] rather than whole brain immersion fixation and we found more robust reactivity for 12E8 in ethanol fixed PiD tissue compared to formalin (data not shown). Our data also suggest glial tau pathology may play an important role in disease progression. We previously found autopsy-confirmed neuroimaging data of selective WM degeneration in FTLD-Tau compared with FTLD-TDP [27] and biochemical experiments find a larger amount of insoluble tau in WM than GM in PiD [30]. Here we also found a reduced MD on MRI in long association tracts (Figure 8) and significant glial tau pathology, both in GM ramified astrocytes and GM/WM oligodendrocytes. Interestingly, we found that the majority of astrocytic tau inclusions in sporadic cases were 3R tau-positive and 4R tau-negative (Figure 3C, D). A previous study reported that astrocytic tau inclusions in PiD are predominantly 4R tau-positive;[44] however, this study included a limited survey of only 3 cases. We confirmed our observations using two 4R tau-specific antibodies (Supplementary Tables 8,9). This finding suggests astrocytes undergo the same 3R tau isoform-specific degenerative process as neighboring neurons in sporadic PiD. It is not clear if astrocytic pathology is an early event from our data, as suggested by some [40]. Mature tau markers were less common in glial cells and WM and we did find a high burden of glial pathology in some Phase I defining regions (MFC, OFC) but not others (CA, DG, AMY) (Supplementary Table 2); thus, there may be regional predilections for glial tau accumulation.

Our neuroimaging findings largely mirrored the literature and our proposed phases of tau neuropathology. We find progressive spread of GM and WM degeneration, beginning in limbic and neocortical frontotemporal regions and then involving subcortical structures. However, there were a few distinctions. MRI data finds relatively mild baseline HIPP

atrophy compared with other limbic regions and MOT atrophy in excess of GP, THAL and SENS atrophy at follow-up scan. This may be due to technical issues of MRI segmentation of medial temporal lobe and regional differences in vulnerability to tau-mediated neurodegeneration. Indeed, we found less neuronal loss microscopically in ANG, SENS, GP, CA and DG despite the early accumulation of tau pathology (Figure 6A) similar to a previous report[4]. Some suggest tau deposition in PiD is not correlated to neuronal loss [45]; while we found tau deposition was highly associated with neuronal loss for most other regions. Sample size and methodological issues may contribute to these discrepancies It is also possible different regions accumulate tau neuropathology at differing rates. Finally, rare autopsy-confirmed MRI studies suggest asymmetric atrophy in PiD[46] which could influence our results. We sample alternating hemispheres at autopsy[9] which reduces sampling bias and only 3 cases (#9, 10, 13) had asymmetric atrophy on gross examination thereby suggesting there may be less asymmetry at end stage PiD when atrophy is most severe. We averaged our hemisphere data for MRI analysis to account for random hemisphere sampling at autopsy. Thus, future studies are required to clarify the selective regional vulnerability to various species of pathogenic tau, and we suggest future staging efforts should incorporate both markers of tau deposition and neuron loss in bilateral hemispheres of autopsy-confirmed samples.

This study has several limitations. Although this is one of the largest and most well-annotated PiD autopsy cohorts reported the number of patients in each phase was relatively small in comparison to more common neurodegenerative diseases [47, 48]. One series of PiD cases included >50 cases, but examined only the hippocampus [49]. Our cases were evaluated by tertiary academic centers, and thus there may be referral bias for atypical or severe disease. Current population-based registry efforts by an ongoing NIH-funded multi-center observational study (NCT02365922) are crucial to obtain population-based data for PiD and other forms of FTLD. We included 2 cases with *MAPT p.*Leu266Val mutations, both of which had severe Phase IV pathology and thus these two cases did not influence our definitions of tau phases, but it is not clear if these cases would show the same regional patterns of tau pathology in milder stages of disease. Finally, there are inherent limitations in drawing conclusions on progression of disease from retrospective cross-sectional autopsy data. As such, we used a comprehensive approach incorporating deep phenotypic information to provide converging evidence for our observations. Future, prospective studies using novel tau imaging ligands [50] and other FTLD-specific biomarkers will be helpful to validate the proposed phases of progression proposed here.

In summary, these data provide novel insights into the progression of PiD neuropathology, which has important implications for FTLD biomarker development and animal models of tau transmission that are critical for testing emerging disease-modifying therapies.

Supplementary Material

Refer to Web version on PubMed Central for supplementary material.

Acknowledgments

We would like to thank the patients and their families, for without their meaningful contributions to research this work would not be possible. We would also like to thank Drs. Heiko Braak and Kelly Del Tredici for their assistance and expertise in preparing the 70 μm thick sections and the late Dr. Les I Binder for the Tau C3 Mab. We thank Mary Leonard for her assistance. This study is supported by NIH grants NS044266, AG038490, AG015116, AG010124, P01NS053488, P01AG032953, P01AG017586, AG043503, NS088341, P01AG019724, P50AG023501 and the Wyncote Foundation.

Abbreviations

PiD	Pick's disease
MTBD	microtubule binding domain
FTLD	frontotemporal lobar degeneration
FTD	frontotemporal dementia
bvFTD	behavioral-variant FTD
PPA	primary progressive aphasia
CBS	corticobasal syndrome
IHC	immunohistochemistry
MAb	monoclonal antibody
ThS	Thioflavin S
UBQ	ubiquitin
GFAP	glial fibrillary associated protein
MAP2	microtubule-associated protein
AMY	amygdala
HIPP	hippocampus
ERC	entorhinal cortex-hippocampus
CA	cornu ammonis-hippocampus
DG	dentate gyrus-hippocampus
ACG	anterior cingulate gyrus
OFC	orbitofrontal cortex
MFC	mid-frontal cortex
SMT	superior-mid temporal cortex
ANG	angular gyrus
SENS	sensory cortex
STR	striatum
MOT	motor cortex

VIS	visual cortex
GP	globus pallidus
THAL	thalamus
MED	medulla
CB	cerebellum
CSC	cervical spinal cord
MBSN	midbrain substantia nigra
MBRN	midbrain red nucleus
LC	locus coeruleus
RPN	raphe nuclei
MEDXII	hypoglossal nucleus
MEDX	dorsal motor nucleus vagus
MEDRF	reticular formation-medulla
MEDIO	inferior olive
MED ARC/PN	arcuate nucleus/pontobulbar body
CBDG	cerebellar dentate gyrus
CBGL	cerebellar granule layer
WM	white matter
MRI	magnetic resonance imaging
ROIs	regions of interest
MD	mean diffusivity
CNS	central nervous system
PBs	Pick bodies
NTs	neuropil threads

References

1. Pick A. Über die Beziehungen der senilen Hirnatrophie zur Aphasie. Prag Med Wochenschr. 1892; 17:165–7.
2. Kertesz A. Pick complex--historical introduction. Alzheimer disease and associated disorders. 2007 Oct-Dec;21(4):S5–7. [PubMed: 18090424]
3. Mackenzie IR, Neumann M, Bigio EH, et al. Nomenclature and nosology for neuropathologic subtypes of frontotemporal lobar degeneration: an update. Acta neuropathologica. 2010 Jan; 119(1): 1–4. [PubMed: 19924424]
4. Yokota O, Tsuchiya K, Arai T, et al. Clinicopathological characterization of Pick's disease versus frontotemporal lobar degeneration with ubiquitin/TDP-43-positive inclusions. Acta neuropathologica. 2009 Apr; 117(4):429–44. [PubMed: 19194716]

5. Piguet O, Halliday GM, Reid WG, et al. Clinical phenotypes in autopsy-confirmed Pick disease. Neurology. 2011 Jan 18; 76(3):253–9. [PubMed: 21242493]
6. Rascovsky K, Hodges JR, Knopman D, et al. Sensitivity of revised diagnostic criteria for the behavioural variant of frontotemporal dementia. Brain : a journal of neurology. 2011 Sep; 134(Pt 9): 2456–77. [PubMed: 21810890]
7. Gorno-Tempini ML, Hillis AE, Weintraub S, et al. Classification of primary progressive aphasia and its variants. Neurology. 2011 Mar 15; 76(11):1006–14. [PubMed: 21325651]
8. Dickson, D., editor. Sporadic Tauopaties: Pick's disease, corticobasal degeneration, progressive supranuclear palsy and argyrophilic grain disease. 2. NY, NY: Cambridge University Press; 2004.
9. Toledo JB, Van Deerlin VM, Lee EB, et al. A platform for discovery: The University of Pennsylvania Integrated Neurodegenerative Disease Biobank. Alzheimer's & dementia : the journal of the Alzheimer's Association. 2014; 10(4):477–84.
10. Montine TJ, Phelps CH, Beach TG, et al. National Institute on Aging-Alzheimer's Association guidelines for the neuropathologic assessment of Alzheimer's disease: a practical approach. Acta neuropathologica. 2012 Jan; 123(1):1–11. [PubMed: 22101365]
11. Van Deerlin VM, Forman MS, Farmer JM, et al. Biochemical and pathological characterization of frontotemporal dementia due to a Leu266Val mutation in microtubule-associated protein tau in an African American individual. Acta neuropathologica. 2007 Apr; 113(4):471–9. [PubMed: 17072625]
12. Hogg M, Grujic ZM, Baker M, et al. The L266V tau mutation is associated with frontotemporal dementia and Pick-like 3R and 4R tauopathy. Acta neuropathologica. 2003 Oct; 106(4):323–36. [PubMed: 12883828]
13. Feldengut S, Del Tredici K, Braak H. Paraffin sections of 70–100 mum: a novel technique and its benefits for studying the nervous system. Journal of neuroscience methods. 2013 May 15; 215(2): 241–4. [PubMed: 23537935]
14. Mercken M, Vandermeeren M, Lubke U, et al. Monoclonal antibodies with selective specificity for Alzheimer Tau are directed against phosphatase-sensitive epitopes. Acta neuropathologica. 1992; 84(3):265–72. [PubMed: 1384266]
15. Brettschneider J, Del Tredici K, Irwin DJ, et al. Sequential distribution of pTDP-43 pathology in behavioral variant frontotemporal dementia (bvFTD). Acta neuropathologica. 2014 Mar; 127(3): 423–39. [PubMed: 24407427]
16. Seubert P, Mawal-Dewan M, Barbour R, et al. Detection of phosphorylated Ser262 in fetal tau, adult tau, and paired helical filament tau. The Journal of biological chemistry. 1995 Aug 11; 270(32):18917–22. [PubMed: 7642549]
17. Hasegawa M, Fujiwara H, Nonaka T, et al. Phosphorylated alpha-synuclein is ubiquitinated in alpha-synucleinopathy lesions. The Journal of biological chemistry. 2002 Dec 13; 277(50):49071–6. [PubMed: 12377775]
18. de Silva R, Lashley T, Gibb G, et al. Pathological inclusion bodies in tauopathies contain distinct complements of tau with three or four microtubule-binding repeat domains as demonstrated by new specific monoclonal antibodies. Neuropathology and applied neurobiology. 2003 Jun; 29(3): 288–302. [PubMed: 12787326]
19. Dan A, Takahashi M, Masuda-Suzukake M, et al. Extensive deamidation at asparagine residue 279 accounts for weak immunoreactivity of tau with RD4 antibody in Alzheimer's disease brain. Acta neuropathologica communications. 2013; 1:54. [PubMed: 24252707]
20. Guillozet-Bongaarts AL, Garcia-Sierra F, Reynolds MR, et al. Tau truncation during neurofibrillary tangle evolution in Alzheimer's disease. Neurobiology of aging. 2005 Jul; 26(7): 1015–22. [PubMed: 15748781]
21. Irwin DJ, Cohen TJ, Grossman M, et al. Acetylated tau neuropathology in sporadic and hereditary tauopathies. The American journal of pathology. 2013 Aug; 183(2):344–51. [PubMed: 23885714]
22. Irwin DJ, Cohen TJ, Grossman M, et al. Acetylated tau, a novel pathological signature in Alzheimer's disease and other tauopathies. Brain : a journal of neurology. 2012 Mar; 135(Pt 3): 807–18. [PubMed: 22366796]

23. Igaz LM, Kwong LK, Lee EB, et al. Dysregulation of the ALS-associated gene TDP-43 leads to neuronal death and degeneration in mice. The Journal of clinical investigation. 2011 Feb; 121(2): 726–38. [PubMed: 21206091]
24. Volpicelli-Daley LA, Luk KC, Patel TP, et al. Exogenous alpha-synuclein fibrils induce Lewy body pathology leading to synaptic dysfunction and neuron death. Neuron. 2011 Oct 6; 72(1):57–71. [PubMed: 21982369]
25. Montine, TJ.; Monsell, SE.; Beach, TG., et al. Alzheimer's & dementia : the journal of the Alzheimer's Association. 2015. Multisite assessment of NIA-AA guidelines for the neuropathologic evaluation of Alzheimer's disease. in press
26. Uchihara, T.; Tsuchiya, K. Neuropathology of Pick body disease. In: Vinken, PJ.; Bruyn, GW., editors. Handbook of clinical neurology. Vol. 89. 2008. p. 415-30.
27. McMillan C, Irwin D, Avants B, et al. White Matter Imaging Helps Dissociate Tau from TDP-43 in Frontotemporal Lobar Degeneration. Journal of neurology, neurosurgery, and psychiatry. 2013; 84(9):949–55.
28. Mori S, Oishi K, Jiang H, et al. Stereotaxic white matter atlas based on diffusion tensor imaging in an ICBM template. NeuroImage. 2008 Apr 1; 40(2):570–82. [PubMed: 18255316]
29. Feany MB, Mattiace LA, Dickson DW. Neuropathologic overlap of progressive supranuclear palsy, Pick's disease and corticobasal degeneration. Journal of neuropathology and experimental neurology. 1996 Jan; 55(1):53–67. [PubMed: 8558172]
30. Zhukareva V, Mann D, Pickering-Brown S, et al. Sporadic Pick's disease: a tauopathy characterized by a spectrum of pathological tau isoforms in gray and white matter. Annals of neurology. 2002 Jun; 51(6):730–9. [PubMed: 12112079]
31. Probst A, Tolnay M, Langui D, Goedert M, Spillantini MG. Pick's disease: hyperphosphorylated tau protein segregates to the somatoaxonal compartment. Acta neuropathologica. 1996 Dec; 92(6): 588–96. [PubMed: 8960316]
32. Armstrong MJ, Litvan I, Lang AE, et al. Criteria for the diagnosis of corticobasal degeneration. Neurology. 2013 Jan 29; 80(5):496–503. [PubMed: 23359374]
33. Berry RW, Sweet AP, Clark FA, et al. Tau epitope display in progressive supranuclear palsy and corticobasal degeneration. J Neurocytol. 2004 May; 33(3):287–95. [PubMed: 15475684]
34. Guillozet-Bongaarts AL, Glajch KE, Libson EG, et al. Phosphorylation and cleavage of tau in non-AD tauopathies. Acta neuropathologica. 2007 May; 113(5):513–20. [PubMed: 17357802]
35. Schmidt ML, Schuck T, Sheridan S, et al. The fluorescent Congo red derivative, (trans, trans)-1-bromo-2,5-bis-(3-hydroxycarbonyl-4-hydroxy)styrylbenzene (BSB), labels diverse beta-pleated sheet structures in postmortem human neurodegenerative disease brains. The American journal of pathology. 2001 Sep; 159(3):937–43. [PubMed: 11549586]
36. Miki Y, Mori F, Tanji K, et al. An autopsy case of incipient Pick's disease: immunohistochemical profile of early-stage Pick body formation. Neuropathology : official journal of the Japanese Society of Neuropathology. 2014 Aug; 34(4):386–91. [PubMed: 24444359]
37. Hornberger M, Piguet O. Episodic memory in frontotemporal dementia: a critical review. Brain : a journal of neurology. 2012 Mar; 135(Pt 3):678–92. [PubMed: 22366790]
38. Towfighi J. Early Pick's disease. A light and ultrastructural study. Acta neuropathologica. 1972; 21(3):224–31. [PubMed: 5056008]
39. Sparks DL, Danner FW, Davis DG, Hackney C, Landers T, Coyne CM. Neurochemical and histopathologic alterations characteristic of Pick's disease in a non-demented individual. Journal of neuropathology and experimental neurology. 1994 Jan; 53(1):37–42. [PubMed: 8301318]
40. Mimuro M, Yoshida M, Miyao S, Harada T, Ishiguro K, Hashizume Y. Neuronal and glial tau pathology in early frontotemporal lobar degeneration-tau, Pick's disease subtype. Journal of the neurological sciences. 2010 Mar 15; 290(1–2):177–82. [PubMed: 20022024]
41. Seeley WW, Crawford R, Rascovsky K, et al. Frontal paralimbic network atrophy in very mild behavioral variant frontotemporal dementia. Archives of neurology. 2008 Feb; 65(2):249–55. [PubMed: 18268196]
42. Kim EJ, Sidhu M, Gaus SE, et al. Selective frontoinsular von Economo neuron and fork cell loss in early behavioral variant frontotemporal dementia. Cerebral cortex. 2012 Feb; 22(2):251–9. [PubMed: 21653702]

43. Seeley WW, Carlin DA, Allman JM, et al. Early frontotemporal dementia targets neurons unique to apes and humans. Annals of neurology. 2006 Dec; 60(6):660–7. [PubMed: 17187353]
44. Arai T, Ikeda K, Akiyama H, et al. Distinct isoforms of tau aggregated in neurons and glial cells in brains of patients with Pick's disease, corticobasal degeneration and progressive supranuclear palsy. Acta neuropathologica. 2001 Feb; 101(2):167–73. [PubMed: 11271372]
45. Kersaitis C, Halliday GM, Kril JJ. Regional and cellular pathology in frontotemporal dementia: relationship to stage of disease in cases with and without Pick bodies. Acta neuropathologica. 2004 Dec; 108(6):515–23. [PubMed: 15368070]
46. Whitwell JL, Josephs KA, Rossor MN, et al. Magnetic resonance imaging signatures of tissue pathology in frontotemporal dementia. Archives of neurology. 2005 Sep; 62(9):1402–8. [PubMed: 16157747]
47. Braak H, Braak E. Neuropathological stageing of Alzheimer-related changes. Acta neuropathologica. 1991; 82(4):239–59. [PubMed: 1759558]
48. Brettschneider J, Del Tredici K, Toledo JB, et al. Stages of pTDP-43 pathology in amyotrophic lateral sclerosis. Annals of neurology. 2013; 74(1):20–38. [PubMed: 23686809]
49. Kovacs GG, Rozemuller AJ, van Swieten JC, et al. Neuropathology of the hippocampus in FTLD-Tau with Pick bodies: A study of the BrainNet Europe Consortium. Neuropathology and applied neurobiology. 2013; 39(2):166–78. [PubMed: 22471883]
50. Maruyama M, Shimada H, Suhara T, et al. Imaging of tau pathology in a tauopathy mouse model and in Alzheimer patients compared to normal controls. Neuron. 2013 Sep 18; 79(6):1094–108. [PubMed: 24050400]

Pt#	Clinical Phen-otype	Age Onset (y)	Age Death (y)	Dis Dur (y)	SEX	Brain Wt. (g)	BRAAK	CERAD	PHASE	AMY	ERC	DG	CA	ACG	OFC	MFC	SMT	ANG	SENS	STR	GP	THAL	MBSN	MBRN	LC	RPN	MEDRF	MEDX	CBDG	CSC	MOT	MEDIO	MEDARC/PB	MEDXII	VIS	CBGL
1	bvFTD	62	68	6	M	1360	1	A	1	2	2	2	2	2	2	2	2	1	-	0	0	0	0	0	0	0	0	0	0	0	0	0	0	0	0	0
2	bvFTD	71	74	3	M	1240	1	0	2	2	2	-	2	3	1	2	1	2	2	2	-	1	1	-	2	1	0	1	0	0	0	0	0	0	0	0	0
3	bvFTD	55	61	6	M	-	1	0	2	2	3	3	3	2	3	3	1	1	-	2	-	1	1	1	2	-	1	-	0	-	0	0	0	-	0	0
4	bvFTD	57	62	5	F	920	0	0	2	2	3	3	3	3	-	3	2	2	-	0	0	0	-	-	2	2	0	0	1	1	0	0	0	0	0	0
5	bvFTD	64	72	8	M	1126	1	A	3	-	-	-	-	3	3	3	-	-	1	3	-	-	2	2	2	-	2	1	-	1	1	1	0	0	0	0
6	CBS/ naPPA	75	81	6	F	1030	0	0	3	3	2	3	3	2	3	-	2	2	-	1	1	1	1	1	3	2	1	1	1	1	2	0	1	0	0	0
7‡	bvFTD	50	61	11	F	1012	0	0	3	3	2	3	2	3	3	3	3	2	0	2	0	2	2	0	2	1	1	1	1	1	1	0	0	0	0	0
8	bvFTD	54	58	4	M	1266	0	0	3	3	2	3	3	3	3	2	1	-	0	2	1	1	0	0	3	2	1	2	0	0	3	0	1	0	0	0
9	bvFTD	58	71	13	M	941	0	0	4	3	3	3	3	3	3	-	3	-	3	3	2	2	2	1	-	3	3	3	3	-	3	1	2	1	1	0
10	bvFTD	63	76	13	M	1021	0	0	4	2	2	3	3	3	2	3	2	1	1	-	-	1	-	-	3	3	1	1	2	1	1	1	2	0	1	0
11	bvFTD	47	59	12	M	793	1	0	4	3	3	2	3	3	2	3	3	1	-	2	-	1	0	0	-	-	0	1	2	0	2	1	1	0	1	0
12	bvFTD	58	62	4	F	1140	0	0	4	3	3	3	3	3	3	-	1	-	2	-	-	2	-	-	-	3	3	2	1	2	3	3	2	1	1	-
13‡‡	CBS/ bvFTD	69	76	7	M	1199	1	B	4	3	3	3	3	3	3	3	3	3	2	3	2	1	1	1	3	3	3	2	-	-	3	1	3	1	1	-
14	bvFTD	61	66	5	M	930	0	0	4	3	3	3	3	3	3	3	3	3	2	3	2	2	2	1	3	3	2	2	2	2	3	2	2	0	1	0
15	bvFTD	47	57	10	M	960	0	0	4	3	3	3	3	3	3	3	2	3	3	-	-	3	-	-	3	3	3	-	-	2	3	1	2	-	1	1
16	AD/ bvFTD	52	67	15	F	788	0	0	4	3	3	3	3	3	3	-	-	2	3	3	-	-	3	3	3	3	-	-	-	3	-	-	-	-	1	0
17*	bvFTD	24	31	7	F	870	1	0	-	3	3	3	3	3	3	3	3	3	2	-	2	3	-	-	3	3	3	3	3	3	3	2	2	1	1	1
18‡‡	bvFTD	73	84	11	F	800	1	C	4	3	3	3	3	3	3		3	2	1	3	1	2	2	2	3	3	2	2	-	1	1	2	2	0	-	0
19	bvFTD	69	84	15	F	914	0	A	4	3	3	3	3	3	3	3	-	3	1	3	2	2	1	0	3	3	2	0	1	2	3	1	2	0	-	0
20†	bvFTD	57	72	14	M	1011	0	0	4	3	3	3	3	3	3	3	3	2	2	3	2	2	2	-	3	-	1	2	2	2	3	0	-	0	0	0
21*†	bvFTD	30	34	5	F	840	0	0	-	3	3	-	3	3	3	3	3	3	-	3	2	3	2	1	3	-	2	2	2	2	2	1	-	1	1	1

Figure 1. Neuropathological Phases of Tau Deposition in PiD

Table demonstrates demographic and neuropathological data for each case. * Denotes pathogenic mutation in MAPT (p.L266V). ‡ secondary pathological diagnoses of Lewy body disease brainstem stage and anoxic encephalopathy, ‡‡ secondary pathological diagnosis of Alzheimer's disease (low probability), † examined using 6 μm sections only. Ordinal scores: (0= none/rare, 1= mild, 2=moderate, 3=severe, -= not done). Braak 1= Braak tau stage I-II.

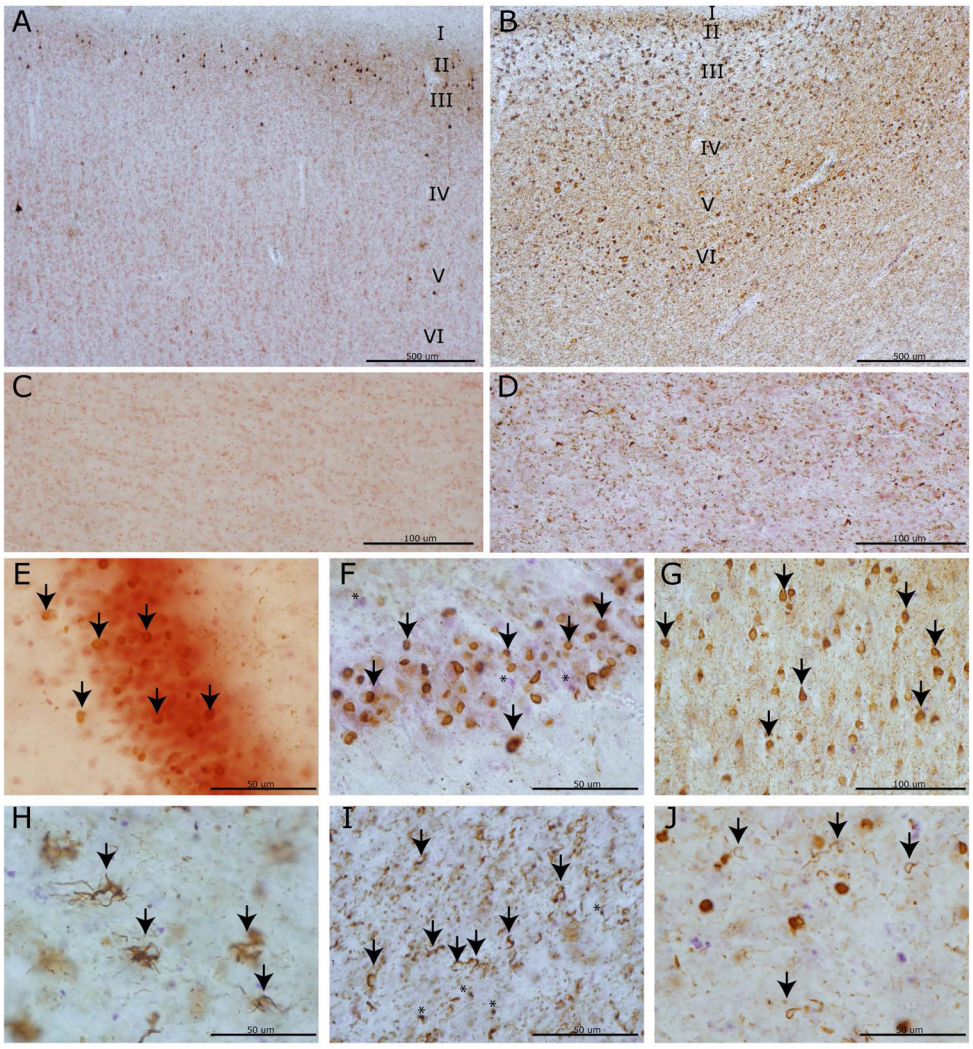

Figure 2. PiD tau pathology and neurodegeneration in cortical and limbic regions

Photomicrographs depict representative images of tau neuropathology (AT-8). A laminar distribution of tau pathology largely restricted to laminae II–III was seen in primary sensory cortex (A) with associated minimal white matter pathology (C) in a Phase II case compared to bi-laminar distribution in anterior cingulate gyrus (B) with layer V–VI involvement and severe white matter tau burden (D) in a Phase IV case. Note the collapse of the cortical layering from severe neuron loss in (B). PBs in dentate gyrus (arrows) in a Phase I case (E) with minimal neuron loss compared to a Phase IV case with mild neuron loss (F; asterisks denote extracellular purple Nissel substance from degenerated neurons). Severe PB burden (arrows) in the cornu ammonis of this hippocampus (G) of a Phase IV case. Glial tau inclusions in the orbitofrontal cortex are depicted (H-J). Ramified astrocytes (arrows) were often present in the orbitofrontal cortex (H). Oligodendrocytic tau pathology in coiled bodies (arrows) is present in both white matter near axonal projections (I) and near soma of affected neurons (J) (i.e. satellite oligodendrocytes) with less common “Pick-body like” oligodendroglial inclusions (I, asterisks).

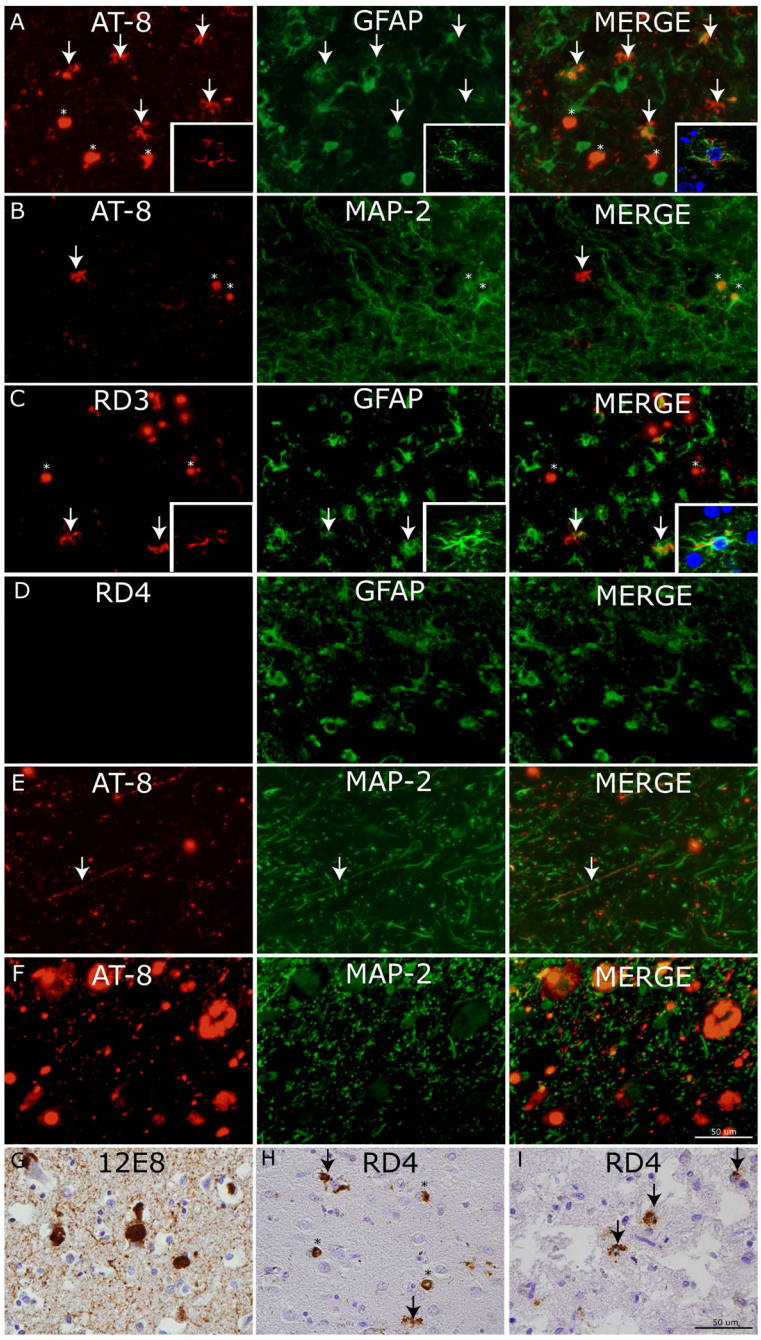

Figure 3. Cellular localization of tau neuropathology

Photomicrographs depict double-label experiments in (A) using anti-phosphorylated tau (AT8) and glial-fibrillary associated protein (GFAP) find ramified astrocytes with tau pathology are largely co-localized with GFAP (arrows) while PBs are not (asterisks) (inset= confocal z-stack images, 63x). Conversely, in (B) AT-8 reactive PBs (asterisks) co-localize with dendritic marker (MAP-2) but ramified astrocytes with tau inclusions do not (arrow). To confirm the major tau isoform composition of tau pathology in ramified astrocytes we performed double label experiments in (C) using 3R tau specific MAb (RD3) and (D) 4R tau

specific MAb (RD4) with GFAP which showed co-localization of GFAP (arrows) with tau inclusions in RD3 but not RD4 double label experiments (inset= confocal z-stack images, 63x). Cervical spinal cord upper Rexed layer tau pathology in (E) and locus coeruleus (F) are seen to co-localize to neuritic processes and cell bodies marked by MAP-2. (G) Robust 12E8 reactivity in PBs and threads in MFC of sporadic PiD. (H) RD4 reactivity was mild and largely found in PBs (asterisks) with occasional nearby ramified astrocyte (arrows). (I) The p.L266V cases showed consistent 4R tau reactive astrocytes (arrows).

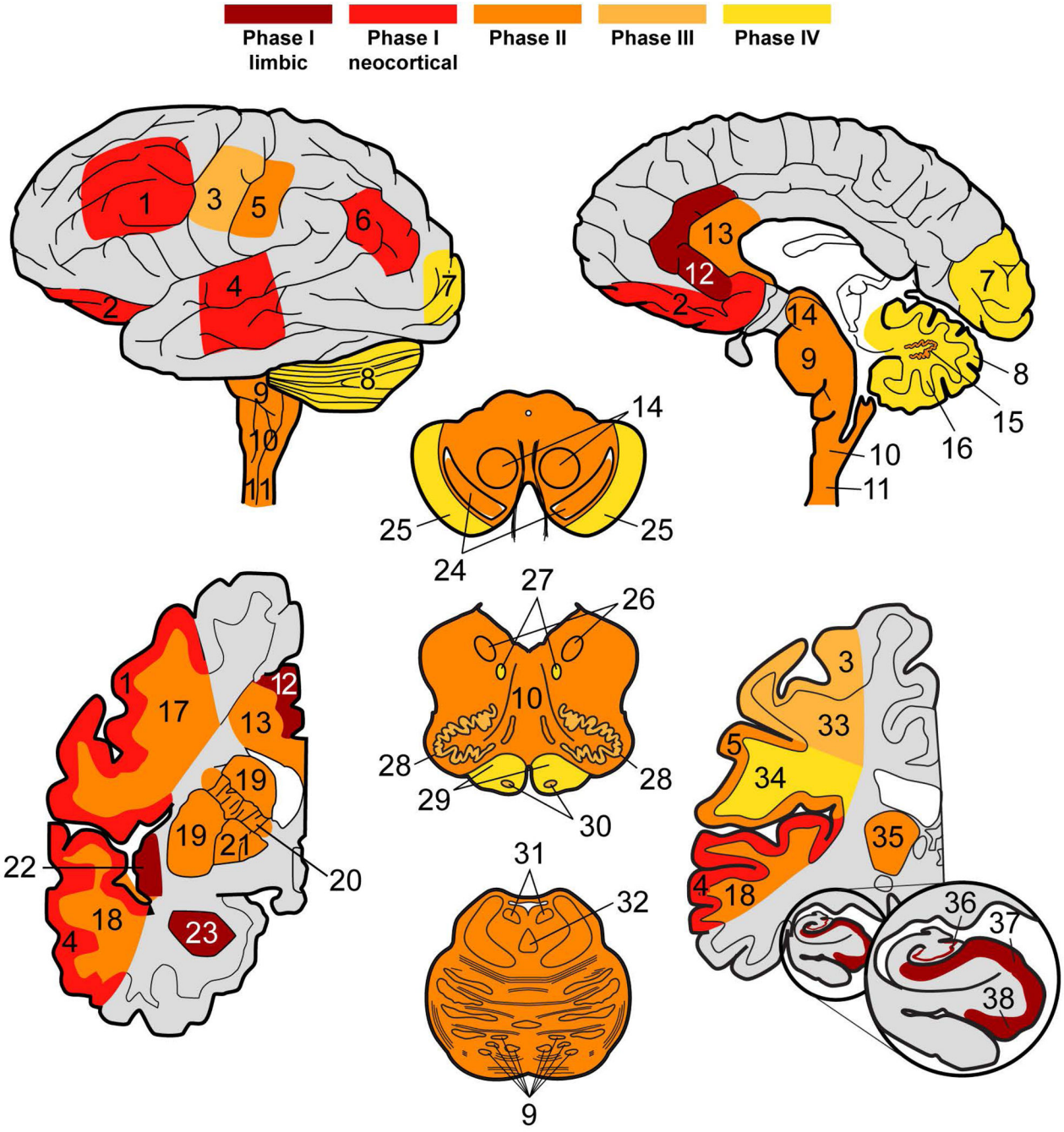

Figure 4. Patterns of PiD tau neuropathology

Heat maps display neuroanatomic associations of sequential tau deposition in the central nervous system of PiD. Phases are defined by the extent of regional involvement of tau pathology across cases beginning with Phase I, where disease is restricted to limbic and neocortical frontotemporal regions and angular gyrus. Phase II has additional pathology in associated white matter tracts, subcortical structures and serotonergic/norandrenergic brainstem nuclei. Phase III tau neuropathology is characterized by additional pathology in primary motor cortex and pre-cerebellar nuclei in the medulla. Finally, Phase IV cases with

the most severe tau pathology burden include additional tau deposits in the visual cortex and variably in the cerebellar granular layer and brainstem white matter. Key: 1=MFC, 2=OFC, 3= MOT, 4=SMT, 5=SENS, 6=ANG, 7=VIS, 8 CBGL, 9=Pons, 10, MEDRF, 11=CSC, 12=ACG, 13=CC, 14=MBRN, 15=CBDG, 16=CB WM, 17= MFC WM, 18= SMT WM, 19=STR, 20= Internal capsule, 21=GP, 22=INS, 23=AMY, 24= MBSN, 25=MB crus cerebri, 26=MEDX, 27=MEDXII, 28=MEDIO, 29=MED pyramids, 30=MED ARC/PB, 31=LC, 32=RPN, 33=MOT WM, 34=SENS WM, 35=THAL, 36= HIPP DG, 37= HIPP CA, 38= HIPP ERC.

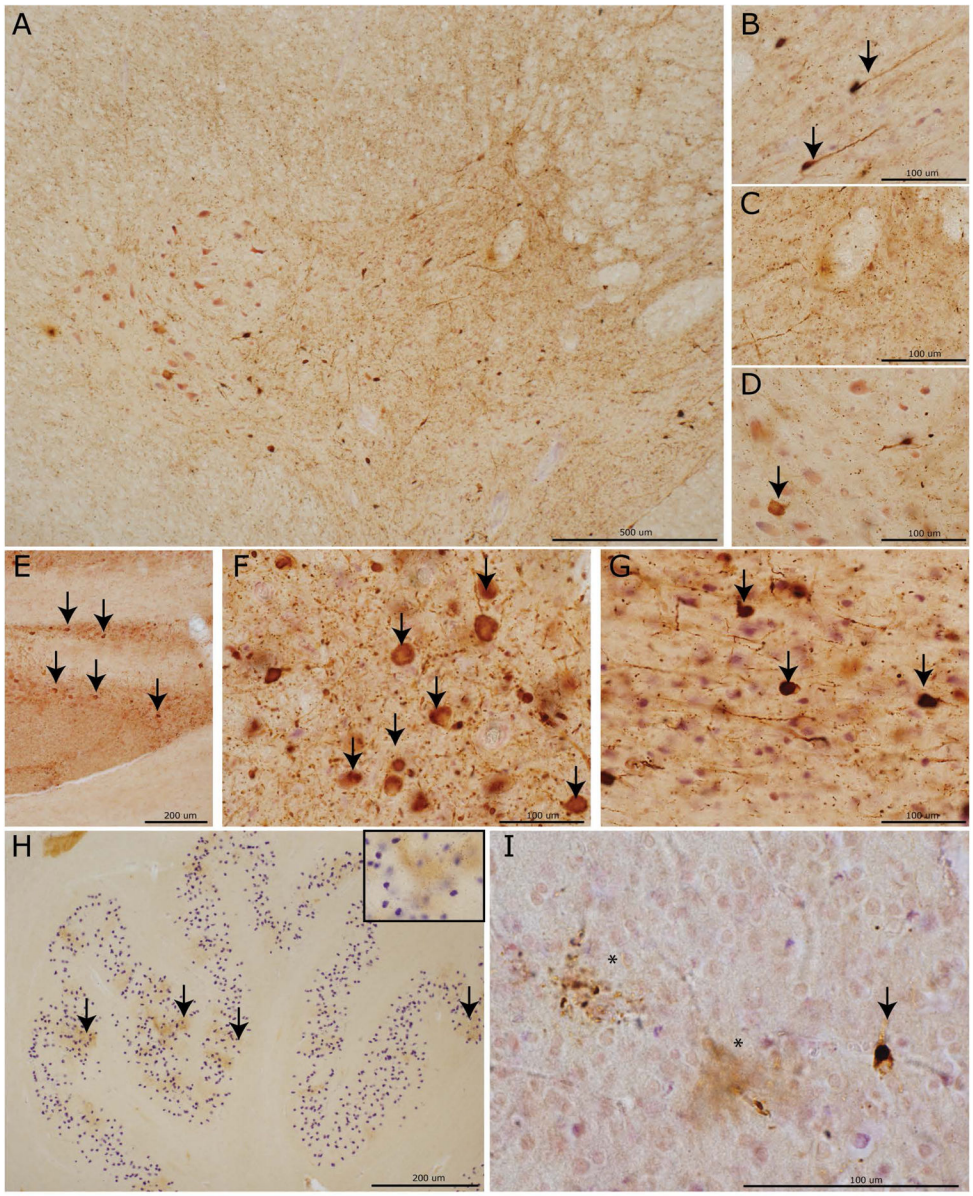

Figure 5. Phase-specific regional tau neuropathology in PiD

Photomicrographs depict representative images from CNS areas sequentially involved in our hypothetical model of the progressive spread of tau pathology in PiD (AT-8). Cervical spinal cord (A) showing a moderate amount of tau neuropathology in the intermediolateral and upper Rexed layers of the spinal cord corresponding to Phase II–IV pathology. High power images reveal neuronal tau inclusions (arrows) in the upper Rexed layers (II–III) (B) and intermediolateral layer (VII) and (D) relative sparing on lower motor neurons (arrow) in layers VIII–IX. Tau inclusions in (E) pontine nuclei in the basis pontis with severe tau pathology (arrows) in the LC (F) and RPN (G) characteristic of Phases II–IV. The inferior olivary pre-cerebellar nucleus (H) with dot-like stippling pattern of tau reactivity (arrows; inset =40x magnification) seen in Phases III–V. Finally, a mild degree of tau positive PBs

(arrows) and diffuse astrocytic tau inclusions (asterisks) in the primary visual cortex (I) representing end-stage Phase IV pathology.

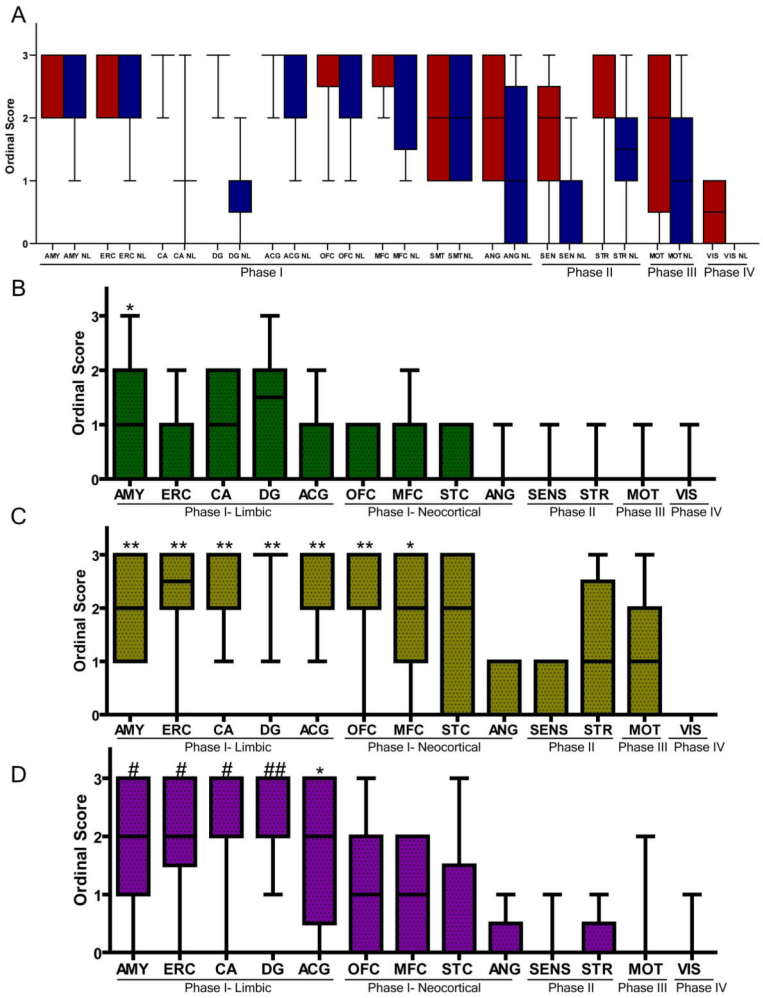

Figure 6. Ordinal scores for severity of regional tau pathology and neurodegeneration in PiD Phases I–IV

Boxplots depict median, interquartile range and range of ordinal scores. (A) AT-8 reactive tau neuropathology (red) in 70 um sections was highly correlated with neuron loss (blue) for most regions. Overall there were higher levels of tau pathology in Phase I regions compared to additional regions affected in Phases II–IV. To further characterize Phase I regions we compared ordinal scores for markers of mature tau pathology. (B) ThS (green) reactivity was mild and most prominent in Phase I limbic regions. (C) The tau C3 C-terminal truncation specific epitope was more abundant in Phase I limbic and neocortical regions. (D) UBQ reactivity was more prominent in Phase I limbic regions. (B–D) K Kruskal-Wallis test finds a significant difference in ordinal scores between regions ($p<0.0001$). * denotes $p<0.001$ difference in post hoc region comparisons with VIS, ** with previous and ANG, SENS, # with previous and STR, MOT, ## with previous and MFC, SMT.

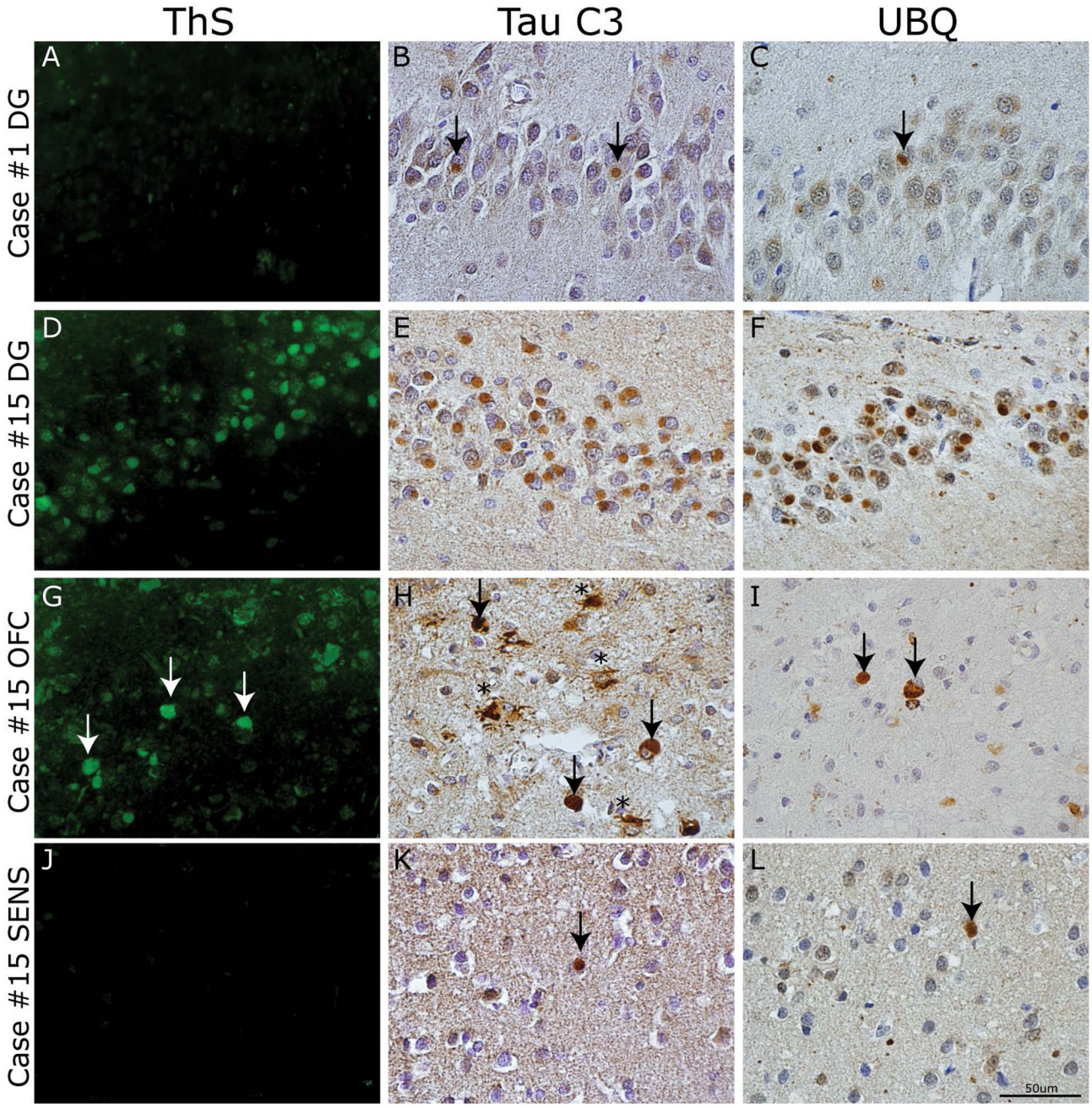

Figure 7. Spatial and temporal gradient of mature tau pathology in PiD

Photomicrographs depict panel of markers of mature tau pathology. Case #1 classified as Phase I had (A) an absence of ThS staining and minimal (B) Tau C3 and (C) UBQ reactivity in the dentate gyrus (arrows). In contrast, case #15 classified as Phase IV had (D) mild to moderate ThS stained PBs in the dentate gyrus of the hippocampus, (G) rare to mild reactivity in OFC (arrows) and (J) rare or no reactivity in SENS. The C-terminal truncation epitope labeled by Tau C3 MAb revealed most consistent tau reactivity in the dentate gyrus (E) and superficial neocortical layer (II–III) pick bodies (arrows) and ramified astrocytes (asterisks) in OFC (H) with mild amounts in SENS (arrow) (K). UBQ-reactive PBs showed

consistent staining in DG (F), with less prominent reactivity in OFC (arrows) (I) and SENS (arrow) (L).

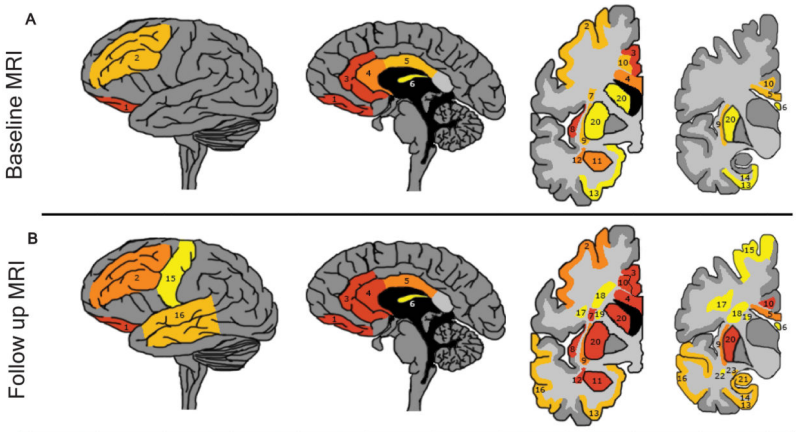

GREY MATTER

ROI Phase	ROI	Key	Baseline MRI	Follow up MRI
I- Limbic	AMY	11	-4.02	-8.07
	HIPP	21	-1.29	-3.00
	ACG	3	-5.92	-7.56
	INS	8	-5.11	-6.47
	ERC	13	-2.24	-3.10
I-Neocortical	OFC	1	-6.73	-6.30
	MFC	2	-3.63	-4.00
	SMT	16	-1.77	-3.19
	ANG	-	-0.72	-1.60
II	STR	20	-2.11	-6.71
	GP	-	1.68	1.43
	THAL	-	1.04	-0.13
	SENS	-	-0.95	-1.20
III	MOT	15	-1.42	-2.63
IV	VIS	-	0.35	-0.51

WHITE MATTER

ROI Phase	ROI	Key	Baseline MRI	Follow up MRI
I-Limbic	GCC	4	-4.35	-7.24
	FOR	6	-2.27	-2.76
	CACG	10	-3.34	-5.38
	CHIPP	14	-2.78	-3.59
	FORST	23	-1.95	-3.99
I-Neocortical	BCC	5	-3.22	-4.16
	AIC	-	-0.85	-1.86
	ACR	7	-3.16	-6.12
	SCR	18	-1.29	-2.01
	PCR	-	-1.13	-1.34
	ILF/FOF	22	-1.56	-2.48
	EXC	9	-3.01	-4.46
	SLF	17	-1.82	-2.19
	SFO	19	-0.78	-2.24
	UNC	12	-4.09	-6.58
II	PIC	-	-1.37	-1.34
	SCC	-	-1.93	-1.81
	ML	-	-1.67	-1.23
III	CST	-	-1.26	0.11
	ICP	-	-0.61	-0.61
	CP	-	-1.66	-0.88
IV	OR	-	-0.95	-1.32
	TAP	-	-0.92	-1.08

Figure 8. Longitudinal antemortem neuroimaging data in PiD

Heat maps depict neuroanatomical regions of interest (ROIs) tested with mean z-scores ≤ −2.0 from autopsied PiD patients (A) at baseline (n=5) and (B) follow up scan (n=4) compared with healthy controls for grey matter density and white matter mean diffusivity. There is time-dependent spread of neurodegeneration from frontal limbic and neocortical regions, largely reflecting proposed hypothetical phases of tau neuropathology based on histopathological analysis of regional tau burden. Key: 1=OFC, 2=MFC, 3=ACG, 4= genu of corpus callosum (GCC), 5= body corpus callosum (BCC), 6= body/column fornix (FOR), 7= anterior corona radiata (ACR), 8= anterior INS, 9= external capsule (EXC), 10= cingulum near ACG (CACG), 11= AMY, 12= uncinate fasciculus (UNC), 13=ERC, 14= cingulum near HIPP (CHIPP), 15= MOT, 16= SMT, 17= superior longitudinal fasciculus (SLF), 18= superior corona radiata (SCR), 19= superior fronto-occipial fasciculus (SFO), 20= STR, 21= HIPP, 22= inferior longitudinal fasciculus/fronto-occipital fasciculus (ILF/FOF). Areas tested and not depicted include fornix crus/stria terminalis (FORST), primary sensory cortex (SENS), angular gyrus (ANG), splenium corpus callosum (SCC), primary visual cortex (VIS), corticospinal tract (CST), medial lemniscus (ML), anterior limb internal capsule (AIC), globus pallidus (GP), thalamus (THAL), cerebral peduncle (CP), posterior

limb internal capsule (PIC). posterior corona radiata (PCR), inferior cerebellar peduncle (ICP), optic radiations (OR) and tapetum (TAP) (z scores all >−2.0).